^{24}Mg(α, γ)^{28}Si resonance parameters at low α-particle energies

E. Strandberg,[*] M. Beard, M. Couder, A. Couture,[†] S. Falahat, J. Görres, P. J. LeBlanc, H. Y. Lee,[‡]
S. O'Brien, A. Palumbo, E. Stech, W. P. Tan, C. Ugalde,[§] and M. Wiescher
University of Notre Dame, Notre Dame, Indiana 46556, USA

H. Costantini
University of Notre Dame, Notre Dame, Indiana 46556, USA and
Istituto Nazionale di Fisica Nucleare, Genova, Italy

K. Scheller
University of Southern Indiana, Evansville, Indiana 47712, USA

M. Pignatari
Keele University, Keele, ST5 5BG, United Kingdom

R. Azuma
University of Toronto, Toronto, Ontario, M5S 1A1, Canada

L. Buchmann
TRIUMF, Vancouver, British Columbia, V6T 2A3, Canada
(Received 13 February 2008; published 5 May 2008)

The reaction ^{24}Mg(α, γ)^{28}Si is involved in the nucleosynthesis of ^{24}Mg and ^{28}Si in massive stars. The reaction has not been examined with sufficient sensitivity at α-particle energies below 1.5 MeV. Several ^{28}Si states appear favorable for formation by this reaction in the α-particle energy range of 1.0–1.5 MeV, motivating a new study of this reaction at the University of Notre Dame. To maximize experimental sensitivity, a high efficiency coincidence detection system was developed. Several previously unknown resonances were observed between 1.1 and 1.5 MeV, and an upper limit for any lower energy resonances was obtained. Resonance parameters were determined and reaction rates were calculated. The astrophysical implications of these results are discussed.

DOI: 10.1103/PhysRevC.77.055801 PACS number(s): 26.20.Np, 24.30.−v, 25.55.−e, 27.30.+t

I. INTRODUCTION

Energy production during stellar carbon burning is based on the ^{12}C(^{12}C,p)^{23}Na(p, α)^{20}Ne and ^{12}C(^{12}C,α)^{20}Ne reactions, which convert most of the ^{12}C fuel into ^{20}Ne. Subsequent α capture on ^{20}Ne produces ^{24}Mg, which is depleted by neutron capture to ^{25}Mg or alternatively converted to ^{28}Si via ^{24}Mg(α, γ)^{28}Si. The abundances of the various magnesium and silicon isotopes depend critically on the interplay of neutron, proton, and α capture reactions in this mass range. Reliable predictions therefore necessitate the determination of the reaction rates of the associated α capture processes for the energy range of stellar carbon burning. From the nucleosynthesis point of view, these considerations are not so important for core carbon burning of massive stars, since this material will become part of a neutron star in the subsequent core collapse. They are, however, particularly important for nucleosynthesis calculations of convective shell carbon burning, since most of the shell material will be ejected during the subsequent shock-driven type II supernova almost unchanged by the explosion.

The goal of this work was to investigate low energy resonances in ^{24}Mg(α, γ)^{28}Si to remove the present uncertainties of the reaction rate. This will allow us to better predict the reaction flow in the convective carbon shell and come to more reliable predictions of the associated nucleosynthesis products of a massive presupernova star. Typical temperatures in the carbon burning shell are $T \approx 1$ GK. This translates to a Gamow energy range of around 1.0–2.0 MeV for the ^{24}Mg(α, γ)^{28}Si reaction. Presently, reliable experimental results exist only down to energies of $E_{\text{c.m.}} \approx 1.3$ MeV, and a full evaluation of the reaction rate at carbon burning temperatures requires extending the measurements to significantly lower temperatures. We will first discuss the previous experimental results, followed by a description of the present experimental setup and the improvements introduced to expand the experimental range toward lower energies. The subsequent section will discuss the analysis of the experimental data and the determination of the strengths of the newly observed resonances. The final section is devoted to the determination of the stellar reaction rate. This

[*]Present address: Lockheed Martin Aeronautics, Palmdale, CA 93599, USA.
[†]Present address: Los Alamos National Laboratory, PO Box 1663, Los Alamos, NM 87545, USA.
[‡]Present address: Argonne National Laboratory, Argonne, IL 60439, USA.
[§]Present address: University of North Carolina, Chapel Hill, NC 27599, USA.

will include not only a discussion of the contribution of the newly observed resonances but also a discussion and estimate of possible additional low energy contributions to the reaction rate. Finally we will evaluate the impact of the new reaction rate on the reaction flux during shell carbon burning.

The first experiment to explore the ^{24}Mg$(\alpha,\gamma)^{28}$Si reaction was performed in 1962 [1]. The lowest energy resonance was observed at 1.529 MeV, with $\omega\gamma = 0.11$ eV and $J^\pi = 1^-$. Nineteen other resonances were observed in the α-particle energy range $E_{\rm lab} = 1.5$–3.2 MeV, most of which could be assigned to states previously known from the ^{27}Al$(p,\gamma)^{28}$Si reaction. The (α,γ) reaction was studied at α-particle energies below 2.8 MeV in 1969 using evaporated Mg targets and beam currents of 2–6 μA [2]. Above 1.5 MeV, the yield curve agreed with the data obtained by Smulders and Endt [1], but an additional feature was discovered at $E \cong 1.35$ MeV. More detailed analysis suggested a resonance at this energy, but the weakness of the resonance precluded a more thorough characterization. A resonance energy of 1.358 ± 0.007 MeV and a resonance strength of 0.0019 eV were assigned. Other groups have since examined the ^{24}Mg$(\alpha,\gamma)^{28}$Si reaction further, but none have studied α-particle energies below 1.5 MeV, either to confirm the resonance found by Lyons [2] or to search for new resonances. With the present experiment, we seek to improve upon the previous data, which were obtained with NaI detectors, by using a combination of high resolution Ge detectors and a high efficiency NaI(Tl) array.

Based on the J^π assignments of known unbound levels in the ^{28}Si nucleus, possible resonances in the (α,γ) channel can be predicted, since resonant α-particle capture by a $J = 0$ nucleus requires a natural parity compound state. Unbound levels with excitation energies around 11 MeV ($E_\alpha = 1.0$–1.5 MeV) are listed in Table I, along with spin and parity values and predictions for formation by the ^{24}Mg$(\alpha,\gamma)^{28}$Si reaction [3].

II. EXPERIMENTAL PROCEDURES

The α-particle beam was supplied by the 3.7 MV KN accelerator at the University of Notre Dame Nuclear Science Laboratory (NSL). The typical beam current on target ranged from 50 to 150 μA. A liquid nitrogen cooled copper tube was mounted in front of the target to reduce carbon deposition. This cold finger was biased to -300 V for secondary electron suppression. The beam was wobbled to produce a homogeneous beam spot size of 1.6×1.0 cm on the target. The target was mounted on a brass target holder and was water cooled, and the target chamber was electrically isolated to allow for charge collection.

TABLE I. Levels of the ^{28}Si nucleus around $E_{\rm ex} = 11$ MeV.

$E_{\rm ex}$ (keV)	J^π	E_α (c.m.) (keV)	E_α (lab) (keV)	Favorable?
10883.45	$2^+(2^-,3^+)$	899.3	1049.1	–
10900.42	1^+	916.2	1068.9	no
10915.7	3^-	931.5	1086.8	yes
10944.0	4^+	959.8	1119.8	yes
10952.8	2^+	968.6	1130.0	yes
10994	$1^+(1^-,2^+)$	1009.8	1178.1	–
11078.52	3^-	1094.3	1276.7	yes
11100.0	6^+	1115.8	1301.8	yes
11142	2^+	1157.8	1350.8	yes
11195.22	4^+	1211.0	1412.9	yes
11242	–	1257.8	1467.4	–
11265.0	3^-	1280.8	1494.3	yes
11295.4	1^-	1311.2	1529.7	yes

The targets were prepared by evaporation of 99.99% pure natural magnesium on 0.02 in. thick copper backings. Copper was chosen for the backing material because of its high thermal conductivity—tests with tantalum backings showed significant surface damage caused by the intense α-particle beam. The backings were pretreated by soaking in a 5% acetic acid solution to improve magnesium adhesion. After evaporation, the targets were immediately transferred to an argon-filled chamber to reduce oxidation of the magnesium coating. Targets were used within one week of production, as oxidation was observed to worsen over time even in the argon environment. Evaporated Mg targets with thicknesses of 100–400 nm were used during the experiment corresponding to target thicknesses of 30– 120 keV at an α beam energy of 1.53 MeV for a target orientation of 45° with respect to the beam direction.

The detection system consisted of four NaI(Tl) detectors and a high-purity germanium clover detector, with the clover operated in add-back mode. The four NaI(Tl) detectors (each 8 in. diameter $\times$6 in. thickness) were mounted in a common stand, and each was rotated 45° in polar and azimuthal angles, with respect to the beam. This arrangement is illustrated in Fig. 1. The stand was placed upstream of the target so that the NaI(Tl) detectors were facing the target. The clover detector was placed at a distance of 2.5 cm behind the target, at 45° with respect to the beam direction to minimize angular distribution effects. The NaI(Tl) stand was placed at 59°, which was the smallest angle attainable before the stand and the beamline collided.

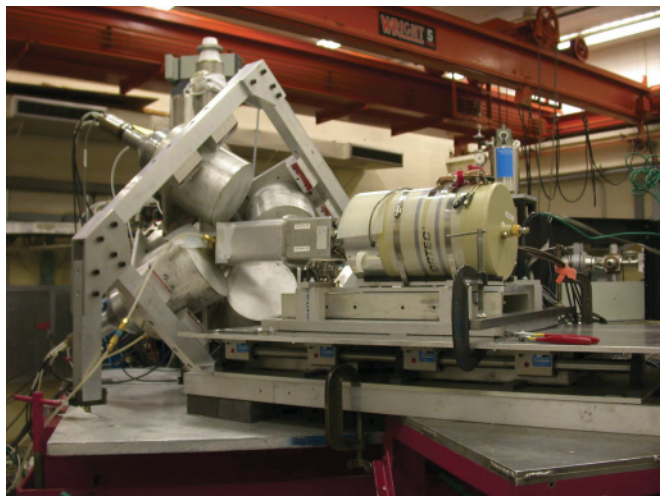

FIG. 1. (Color online) Detection system, consisting of four large NaI(Tl) detectors and a clover Ge detector . In this picture, the beam is directed toward the viewer.

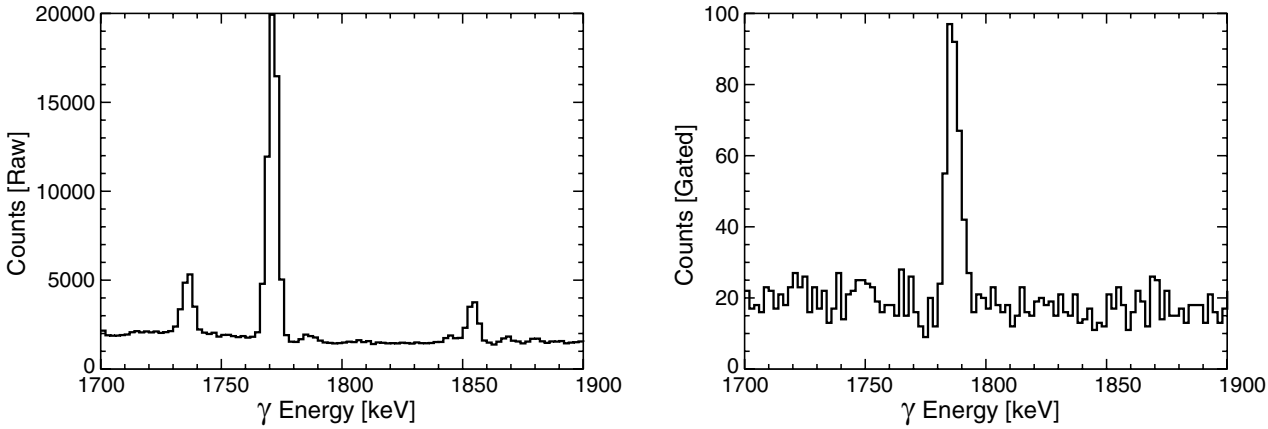

FIG. 2. Clover spectrum of the 1.178 MeV resonance before (left) and after (right) applying coincidence gates. In the left frame, the 1.779 MeV γ-ray line is weak, and the spectrum is dominated by environmental background lines, particularly the 1.764 MeV line from the decay of ^{214}Bi. The background lines are eliminated by applying the coincidence gates, as seen in the right frame.

The detectors were operated in coincidence mode, with the NaI(Tl)'s observing the high energy primary γ-ray decay of the ^{28}Si resonance state, and the clover observing the secondary 1.779 MeV γ-ray transition from the first excited state to the ground state. The trigger for the data acquisition was an event in the germanium detector with energy above the threshold of approximately 0.1 MeV. This essentially created a coincidence requirement for the NaI(Tl) detectors, as their signals would only be acquired if they came in coincidence with a clover signal. This hardware cut was necessary to achieve a reasonable dead time in the data acquisition, due to the high efficiency of the large NaI(Tl) crystals.

Additionally, several software coincidence requirements were employed. A register was used to determine which detectors fired during each event within a 200 ns window, allowing for rejection of random coincidences. A time-to-amplitude converter gate was set to maximize the peak-to-background ratio for the 1.779 MeV γ-ray line. The final coincidence condition was an event above 2.7 MeV in any of the NaI(Tl) detectors. This energy was chosen to not only eliminate most of the environmental background but also include the transition from the second excited state to the first excited state, at 2.839 MeV. This and the other coincidence conditions led to a dramatic reduction in background at 1.779 MeV, and thus greatly increased experimental sensitivity. This is illustrated in Fig. 2. These spectra are from a weak resonance in ^{24}Mg(α, γ)^{28}Si. The peak-to-background ratio of the 1.779 MeV peak is 1.1 in the raw spectrum. While the absolute number of counts is reduced by applying the coincidence requirements, the peak-to-background ratio is improved to 2.7.

The yield curve from the experiment can be seen in Fig. 3. Three new resonances were observed at $E_\alpha = 1.413$, 1.277, and 1.178 MeV. The existence of an expected resonance at 1.130 MeV could not be confirmed, but the data give an upper limit for the resonance strength. The lowest energy point of the yield curve, at 1.065 MeV, was the result of a very long run (>20 C accumulated charge). The target was thick enough to stop the beam in the magnesium layer, leading to an upper limit for all resonances below this beam energy.

III. DATA ANALYSIS

The ^{24}Mg(α, γ)^{28}Si experiment produced a data set consisting of several hundred γ-ray spectra at α-particle energies in the 1.0–1.5 MeV range. The raw data were gated for coincidences, as described in the previous section. The resulting peak at 1.779 MeV in the clover spectra was then analyzed to extract the yield at each experimental energy. To determine the area of the peak, the background was fit with a second-order polynomial function and subtracted from the raw area. The resulting net area I was used to determine the number of ^{28}Si nuclei formed by each incoming α particle, that is,

$$Y_\infty = \frac{Ie}{\mathrm{LQ}\eta\mathrm{BR}}, \tag{1}$$

where LQ is the charge collected during the run, corrected for dead time, η is the detection efficiency, and BR is the percentage of decays that included the 1.779 MeV γ-ray transition. The net area I was corrected for target deterioration;

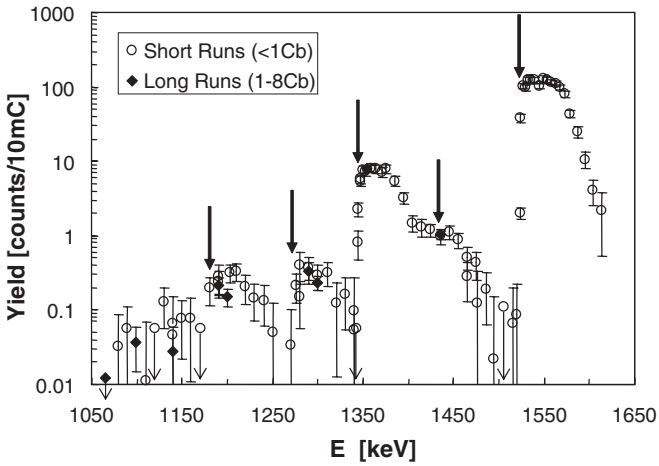

FIG. 3. The yield curve for the ^{24}Mg(α, γ)^{28}Si reaction in the α energy range of 1.05 to 1.65 MeV.

TABLE II. Branching ratios of measured resonances.

Resonances		γ decay to E_{ex} (%)												Source
E_α (keV)	E_{ex} (keV)	0	1.78	4.62	4.98	6.28	6.69	6.88	7.38	7.42	8.26	9.32	9.38	
1087	10916		74 *3*	14 *2*								12 *2*		NuDat [7]
1120	10994		53 *3*						11 *2*	22 *3*	14 *2*			Endt [3]
1130	10953		100											Endt [3]
1178	10994	85 *8*	15 *3*											present exp.
1277	11079		35 *1*			29 *1*				17 *1*		12 *1*	7 *1*	Brenneisen [5]
1351	11142		44 *4*	10 *1*					32 *3*	14 *2*				present exp.
1413	11195		39 *6*	29 5		10 *2*			9 *2*			8 *3*	5 *2*	Endt [8]
1530	11295	73 *5*	19 *2*		2.5 *1.0*		2.2 *1.0*	3.0 *1.0*						present exp.
		75 *8*	21 *2*		<3		2 *1*	2 *1*						Maas *et al.* [6]

after accumulating around 6 C of α-particle beam, the targets generally showed a 20% reduction in yield.

The clover singles efficiency was determined using a ^{60}Co source and the well-known ^{27}Al$(p,\gamma)^{28}$Si resonances at $E_p = 0.992$ and 0.679 MeV. Relative values for the resonance strengths were taken from Endt [3] and were scaled to the 0.992 MeV resonance strength given by Paine and Sargood [4]. The coincidence efficiency is equal to the product of the 1.779 MeV photopeak efficiency in the clover detector and the "total" efficiency to detect the primary γ rays in the NaI(Tl) detectors (this efficiency is not the same as the total efficiency as usually defined, because only γ rays with energy above 2.7 MeV were included). While the 1.779 MeV efficiency of the clover detector is a constant, the NaI(Tl) efficiency varies depending on the energy of the primary γ ray. This energy dependence has been measured using the ^{27}Al$(p,\gamma)^{28}$Si resonances at $E_p = 0.992, 0.760$, and 0.679 MeV, which have decay schemes similar to the ^{24}Mg$(\alpha,\gamma)^{28}$Si resonances.

For several of the ^{24}Mg$(\alpha,\gamma)^{28}$Si resonances measured in this experiment, the decay schemes were completely unknown. Therefore, it was necessary to calculate the branching ratios for these resonances before the resonance strengths could be determined. Additionally, several previous branching ratio measurements were confirmed. The method of calculation was based on Eq. (1). Consider a decay in which three γ rays are observed: (1) the transition from the excited state to the ground state, (2) the transition from the excited state to the first excited state, and (3) the transition from the first excited state to the ground state. If the efficiencies and branching ratios are known, each of the γ-ray lines could be used to calculate the thick target yield Y_∞, and the right-hand side of Eq. (1) can be equated for the three γ rays as

$$\frac{I_1}{\eta_1 \mathrm{BR}_1} = \frac{I_2}{\eta_2\,\mathrm{BR}_2} = \frac{I_3}{\eta_3 \mathrm{BR}_3}. \tag{2}$$

In the simple decay under consideration, BR2 = BR3, and BR1 + BR2 = 1. This system of equations can be solved for BR1 and BR2. Note that the γ-ray yields I_1 and I_2 must be corrected for summing.

The resonance formed at $E_\alpha = 1.178$ MeV corresponds to the ^{28}Si excited state E_{ex} = 10.994 MeV; this state is listed as decaying 100% directly to the ground state [3]. However, in the present experiment, a branching to the first excited state was observed in addition to the ground state transition. For the resonance at E_α = 1.351 MeV, corresponding to the state at $E_{ex} = 11.142$ MeV, branching ratios had not been previously measured. These were easily calculated from the current data, owing to the relatively high resonance strength at this α-particle energy. Branching ratios were not calculated for the resonances at $E_\alpha = 1.277$ MeV ($E_{ex} = 11.079$ MeV) and 1.413 MeV ($E_{ex} = 11.195$ MeV) because the primary γ rays could not be discerned from the clover spectrum, and the values from Brenneisen *et al.* [5] were used. The branching ratios for the well-known $E_\alpha = 1.530$ MeV resonance ($E_{ex} =$ 11.295 MeV) were calculated and found to be in agreement with the branching ratios given by Maas *et al.* [6]. The branching ratios of all the measured resonances are listed in Table II.

The resonance strengths were calculated for each of the observed resonances by combining the two expressions for the thick target yield, Eq. (1) and

$$Y_\infty = \frac{2\pi^2 \lambda\!\!\!^{-}}{\epsilon}\omega\gamma. \tag{3}$$

$\lambda\!\!\!^{-}$ is the de Broglie wavelength of the resonance, and ε is the stopping power of the target; stopping power values were taken from SRIM 2003 [9]. First the resonance strength of the 1.531 MeV resonance was calculated relative to the well-known strength of the 0.992 keV resonance in ^{27}Al$(p,\gamma)^{28}$Si [4] and a value of 0.094 ± 0.014 eV was found. The strengths of the other resonances were calculated relative to this value and are listed in column 2 of Table III. The errors include besides the statistical errors the uncertainties of the reference value (6.9% [4]), stopping powers (5% [9]), relative efficiency (5%), absolute charge measurement (2%), and involved branching ratios (5–20%). The $\omega\gamma$ of the 1.531 MeV resonance agrees within errors with the previous value of 0.110 ± 0.020 eV from Maas *et al.* [6]. The weighted average of these two values of 0.099 ± 0.011 eV was adopted, and the strengths of the other resonance strengths were scaled accordingly (last column in Table III).

Resonance strength upper limits were calculated for two energies where levels exist in the ^{28}Si nucleus, even though resonances were not clearly observed in the yield curve. The

TABLE III. ^{24}Mg(α, γ)^{28}Si resonance strengths.

E_R (MeV)	$\omega\gamma$–this experiment (eV)	$\omega\gamma$-previous value (eV)	$\omega\gamma$-adopted value (eV)
1.530	0.094 ± 0.014	0.110 ± 0.020	0.099 ± 0.011
1.413	$21 \times 10^{-5} \pm 4 \times 10^{-6}$	–	$22 \times 10^{-5} \pm 4 \times 10^{-6}$
1.351	0.0019 ± 0.0003	0.0019 ± 0.0006	0.0020 ± 0.0003
1.277	$58 \times 10^{-5} \pm 11 \times 10^{-5}$	–	$62 \times 10^{-5} \pm 11 \times 10^{-5}$
1.178	$2.2 \times 10^{-4} \pm 6 \times 10^{-5}$	–	$2.3 \times 10^{-4} \pm 6 \times 10^{-5}$
1.120/1.130	$<1.6 \times 10^{-5}$	–	–
1.087	$<1.4 \times 10^{-5}$	–	–
<1.060	$<2 \times 10^{-6}$	–	–

energies are $E_\alpha = 1.120/1.130$ and 1.087 MeV, corresponding to $E_{ex} = 10.944/10.953$ and 10.916 MeV. The thickness of the targets, $\geqslant$30 keV, prohibited differentiation between the possible resonances at 1.120 and 1.130 MeV. In both cases, the feeding probability was set to the maximum value of 1.00; the branchings are listed in Table II. The calculated resonance strength upper limits are $\omega\gamma(1.120/1.130) < 1.6 \times 10^{-5}$ eV and $\omega\gamma(1.087) < 1.4 \times 10^{-5}$ eV.

A target of sufficient thickness to stop the beam in the magnesium layer was used for over 22 C of accumulated charge at a beam energy of 1.060 MeV in order to obtain an upper limit on the strengths of all resonances below this energy. The yield for this run is represented by the lowest energy point in Fig. 3 and is seen to be low compared to the other long run yields, suggesting that there are no strong resonances at energies below 1.060 MeV. Assuming a feeding probability of 1.00, the resonance strength upper limit was found to be $\omega\gamma(E < 1.060) < 2 \times 10^{-6}$ eV. This value could be used to estimate requirements on beam current and detection efficiency for future experiments probing lower α-particle energies.

IV. ASTROPHYSICAL REACTION RATE

The reaction rate was calculated over a temperature range of 0.1–10 GK, including all resonances up to $E_\alpha = 3.792$ MeV; for the newly measured resonances, the new resonance strengths were used, while for all other resonances the strengths were taken from Endt [8]. The reaction rate was compared with several other reaction rate calculations to determine the effect of the newly measured resonance strengths. The rates were taken from Caughlan and Fowler [10] and from Rauscher, Thielemann, Görres, and Wiescher [11]. The latter deals specifically with the capture of α particles by self-conjugated nuclei. The rate of Caughlan and Fowler is derived from measured resonances and suspected resonances in the compound nucleus, as well as nonresonant continuum features. The rates were fit over a temperature range of 0.1–10 GK by least-squares analysis. A comparison of the current experimental rate with these previously calculated rates is shown in Fig. 4. Additionally, the experimental and Caughlan and Fowler rates are tabulated in Table IV. The discrepancy between the current experimental rate and the theoretical rates below 0.3 GK is due to the inclusion of several resonances which are presumed to be present at energies below the range of this experiment.

In addition to the reaction rates of the measured resonances, the theoretical contributions from possible lower energy resonances were examined. The candidate ^{28}Si levels were chosen based on a favorable spin assignment (low J with natural parity); the levels are listed in Table V. The resonance strengths were estimated from a systematic examination of nearby levels. The resonance strength can be written as

$$\omega\gamma = \frac{2J+1}{(2j_1+1)(2j_2+1)}\frac{\Gamma_\alpha\Gamma_\gamma}{\Gamma}. \quad (4)$$

In the case of ^{24}Mg+α, both j_1 and j_2 are zero, simplifying the equation to

$$\omega\gamma = (2J+1)\frac{\Gamma_\alpha\Gamma_\gamma}{\Gamma}. \quad (5)$$

TABLE IV. ^{24}Mg(α, γ)^{28}Si reaction rates (in cm^3/s mol) for 0.1–10 GK.

$T9$ (GK)	Exp.	Ref. [10]
0.1	–	7.93×10^{-31}
0.15	1.11×10^{-32}	8.22×10^{-24}
0.2	2.21×10^{-24}	3.17×10^{-20}
0.3	3.83×10^{-16}	2.76×10^{-15}
0.4	5.08×10^{-12}	3.79×10^{-12}
0.5	1.82×10^{-9}	1.19×10^{-9}
0.6	1.14×10^{-7}	8.69×10^{-8}
0.7	2.50×10^{-6}	2.12×10^{-6}
0.8	2.69×10^{-5}	2.41×10^{-5}
0.9	1.75×10^{-4}	1.61×10^{-4}
1.0	7.96×10^{-4}	7.40×10^{-4}
1.5	8.02×10^{-2}	7.35×10^{-2}
2.0	8.65×10^{-1}	7.98×10^{-1}
2.5	3.86	3.68
3.0	1.11×10^{1}	1.09×10^{1}
3.5	2.48×10^{1}	2.49×10^{1}
4.0	4.67×10^{1}	4.72×10^{1}
4.5	7.75×10^{1}	–
5.0	1.17×10^{2}	1.19×10^{2}
6.0	2.18×10^{2}	2.24×10^{2}
7.0	3.37×10^{2}	3.56×10^{2}
8.0	4.62×10^{2}	5.08×10^{2}
9.0	5.81×10^{2}	6.77×10^{2}
10.0	6.91×10^{2}	8.58×10^{2}

TABLE V. Possible Low Energy ^{24}Mg$(\alpha,\gamma)^{28}$Si Resonances.

E_{ex} (keV)	J^π	E_α (c.m.) (keV)	E_α (lab) (keV)	$\omega\gamma$ (eV)
10514.1	2+	530	618	2.18×10^{-12}
10805.5	2+	822	959	3.55×10^{-7}
10883.5	2+	899	1049	2.95×10^{-6}

If we assume that Γ_γ is much larger than Γ_α, then the resonance strength can be estimated as $\omega\gamma \approx (2J+1)\Gamma_\alpha$. It is not clear that Γ_γ is in fact larger than Γ_α, but the available evidence seems to support this assertion: out of the five nearest ^{28}Si levels for which Γ_γ and Γ_α are known, four have larger γ widths.

The width can be expressed as a function of the penetrability P, the spectroscopic factor θ^2, and the radius of the compound nucleus R_n:

$$\Gamma = \frac{2\hbar}{R_n}\left(\frac{2E}{\mu}\right)^{1/2} P(E, R_n)\theta^2. \quad (6)$$

To estimate a value for θ^2, which is generally determined experimentally, known values for nearby resonances with the same spin were averaged, leading to a value of 0.013 (the range of values was 0.000 025 to 0.044). The α-particle widths and resonance strengths were then calculated. The results are shown in Fig. 5. For comparison, the current experimental rate and the NON-SMOKER rate are shown. The 0.899 MeV resonance appears to be too weak to contribute significantly to the reaction rate. The 0.822 MeV resonance may be the dominant resonance for a small portion of the temperature range. In the lowest part of the temperature range (below $T \approx 0.25$ GK), the 0.530 MeV resonance is likely the largest contributor.

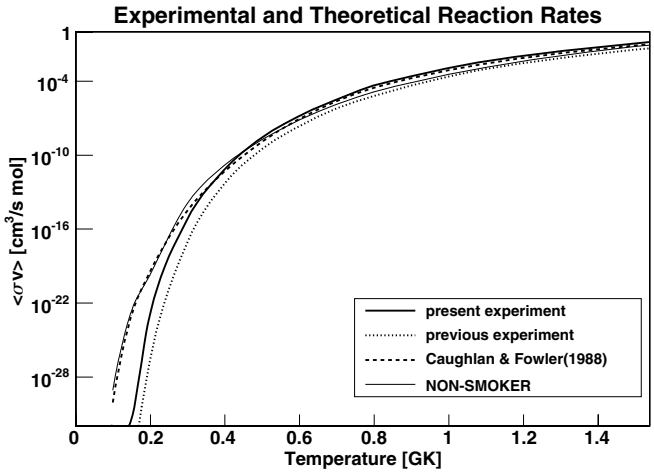

FIG. 4. Two theoretical reaction rates are shown, along with the previous and current experimental rates. The Caughlan and Fowler rate is from Ref. [10], while the previous experimental and NON-SMOKER rates are from Ref. [11].

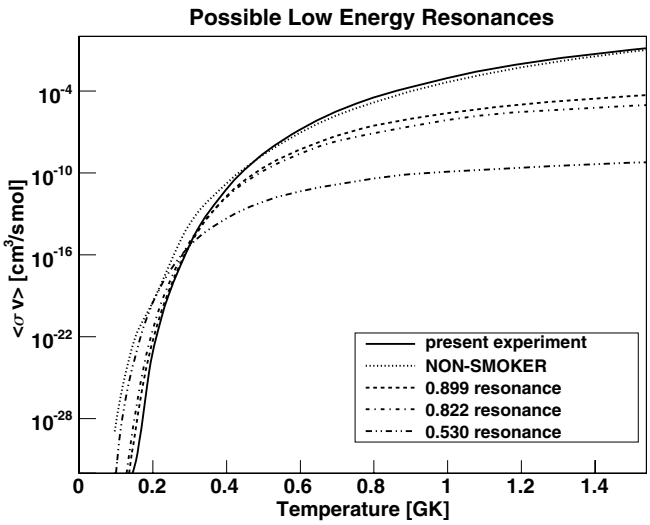

FIG. 5. Projected rates for possible low energy resonances, along with the total rate.

V. ASTROPHYSICAL DISCUSSION

This measurement of the ^{24}Mg$(\alpha,\gamma)^{28}$Si reaction led to the discovery and characterization of several previously unknown resonances in the Gamow energy range of carbon burning. The experimental results reduce significantly the previous uncertainties associated with the ^{24}Mg$(\alpha,\gamma)^{28}$Si reaction rate. Taking into account possible contributions from low energy resonances, the reaction rate is calculated over a wide temperature range. The new results show reasonably good agreement with previous estimates [10,11].

Based on the new experimental rates, we have examined the role of the ^{24}Mg$(\alpha,\gamma)^{28}$Si reaction during the shell carbon burning phase of a solar metallicity $25M_\odot$ star. The C-burning temperature ranges between $T = 1$ and $T = 1.4$ GK, and the typical density is 10^5 cm^{-3} (see also Refs. [12,13]). The nucleosynthesis calculations have been performed by a post-processing code [14,15], where the charged particle reaction rates used in this study are tabulated in NACRE [16] and the neutron capture rates are taken from the KADONIS tables [17]. Figure 6 shows the most important α-particle capture flows compared to ^{24}Mg$(\alpha,\gamma)^{28}$Si in the C shell, where ^{4}He is formed in the ^{12}C(^{12}C,α)^{20}Ne reaction. The most dominant α poison reactions are ^{16}O$(\alpha,\gamma)^{20}$Ne and, initially, ^{22}Ne$(\alpha,n)^{25}$Mg, which is later replaced by ^{20}Ne$(\alpha,\gamma)^{24}$Mg. Both ^{16}O and ^{22}Ne are nucleosynthesis products of the preceding helium burning phase. The ^{24}Mg$(\alpha,\gamma)^{28}$Si reaction plays a rather insignificant role as an α-particle poison during convective shell carbon burning.

The role of the reaction for the nucleosynthesis of ^{24}Mg and ^{28}Si during shell carbon burning is more significant, as demonstrated by Fig. 7. The left-hand panel demonstrates the role of ^{24}Mg$(\alpha,\gamma)^{28}$Si for the nucleosynthesis of ^{24}Mg. Indeed, in massive stars most of ^{24}Mg is produced in convective shell C burning [18]. At carbon ignition at the bottom of the shell, the dominant production process is ^{23}Na$(p,\gamma)^{24}$Mg, with contributions from ^{23}Na$(n,\gamma)^{24}$Na$(\beta^-\nu)^{24}$Mg and ^{20}Ne$(\alpha,\gamma)^{24}$Mg.

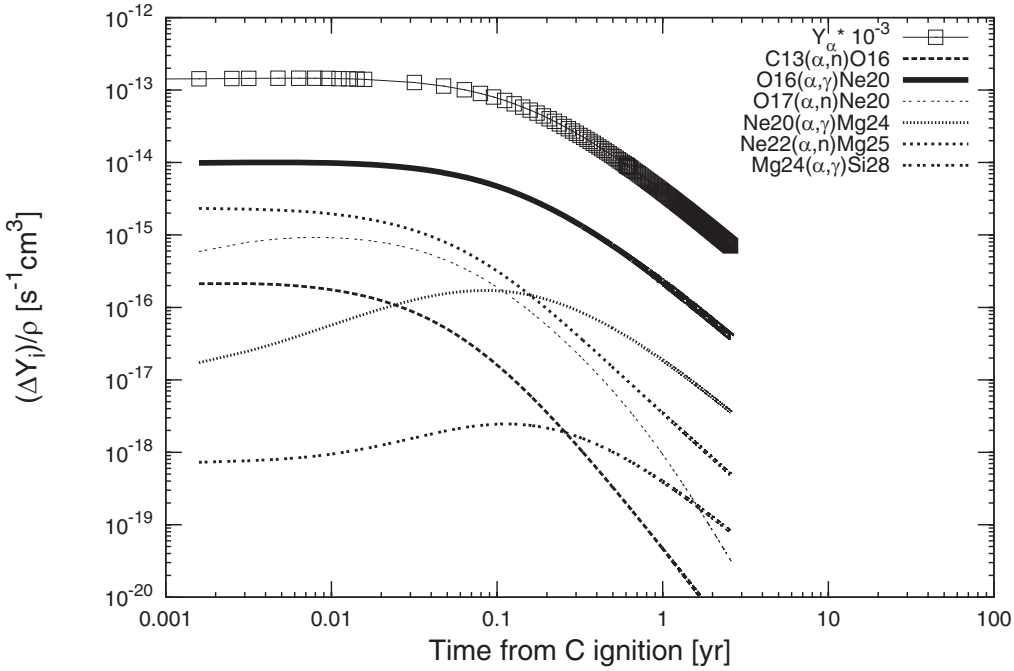

FIG. 6. Comparison of the strengths of all ^{4}He depleting reactions (α poisons) during shell carbon burning. ^{16}O(α, γ)^{20}Ne is the strongest α-particle poison because of the high ^{16}O abundance; ^{24}Mg(α, γ)^{28}Si on the other hand is one of the weakest α-particle poisons. Only toward the end of shell carbon burning does it become stronger as a result of the increase in ^{24}Mg abundance. ΔY_i is the isotopic variation due to the reaction ($Y_i = X_i/A_i$, where X_i is the mass abundance and A_i is the mass number), and ρ is the matter density in cm^{-3} units. The ^{4}He abundance is also reported divided by a factor of 1000 to fit it in the y-axis scale.

The ^{20}Ne(α, γ)^{24}Mg reaction rapidly becomes the strongest production channel, owing to the efficient production of ^{20}Ne during carbon burning. The depletion of ^{24}Mg is dominated by the ^{24}Mg(n, γ)^{25}Mg neutron capture process. The figure demonstrates that this branch is on average more than one order of magnitude larger than the competing α-particle capture ^{24}Mg(α, γ)^{28}Si reaction investigated in this study. Finally, we notice that the ^{24}Mg(p, γ)^{25}Al effect is negligible, because it is

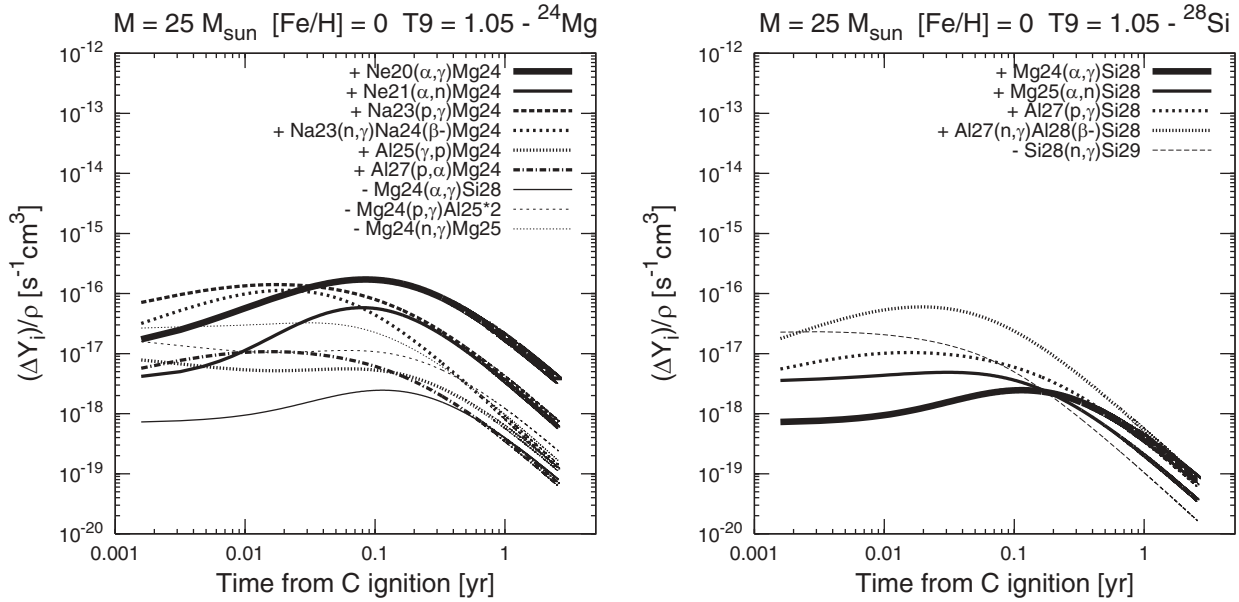

FIG. 7. (Left) strengths of all reactions contributing to the nucleosynthesis of ^{24}Mg during shell carbon burning. The most pronounced production reaction is ^{20}Ne(α, γ)^{24}Mg, and the most prominent depletion process is ^{24}Mg(n, γ)^{25}Mg. (Right) strengths of all reactions contributing to the nucleosynthesis of ^{28}Si during shell carbon burning. The strongest production reaction is induced by neutron capture ^{27}Al(n, γ)^{28}Si($\beta\nu$)^{28}Si, and the dominant depletion process is the neutron capture ^{28}Si(n, γ)^{29}Si.

instantaneously followed by the opposite photodisintegration ^{25}Al(γ, p)^{24}Mg.

After carbon burning, the following evolutionary phase is Ne burning where the photodisintegration ^{20}Ne(γ, α)^{16}O efficiently depletes ^{20}Ne producing α particles beyond $T9 = 1.5$. Most of the α particles are captured in the nucleosynthesis chain ^{20}Ne(α, γ)^{24}Mg(α, γ)^{28}Si, which regulates also the ^{24}Mg nucleosynthesis (e.g., Ref. [19]). However the Ne core material is processed by the following evolutionary phases in which ^{24}Mg is depleted, first by the O burning, and according to the present stellar models, it is not ejected by the final supernova explosion (e.g., Ref. [18]). In case a convective Ne shell is developed and it is unaffected by the more advanced burning phases, it will be strongly processed by the final supernova explosion. The right-hand panel of Fig. 7 shows the main reaction flows responsible for the nucleosynthesis of ^{28}Si in the C burning shell. The ^{24}Mg(α, γ)^{28}Si reaction becomes important toward the final phase of carbon burning after a substantial ^{24}Mg abundance has been built up in the nucleosynthesis process. In massive stars, ^{28}Si is mainly produced in oxygen burning conditions, via ^{16}O(^{16}O,α)^{28}Si and ^{16}O(^{16}O, p)^{31}P(p, α)^{28}Si [20]. In these regions, its final abundance is affected by explosive nucleosynthesis. Additionally, ^{28}Si is partially produced in the previous phases of neon burning and carbon burning. The calculation suggests that the dominant production process is ^{27}Al(n, γ)^{28}Al($\beta\nu$)^{28}Si, followed by ^{27}Al(p, γ)^{28}Si and ^{25}Mg(α, n)^{28}Si.

Figure 8 shows the abundance evolution of ^{12}C, ^{20}Ne, ^{24}Mg, and ^{28}Si in the convective carbon shell as a function of time starting from carbon ignition (see also Ref. [21]). The initial abundance distribution is the result of the previous helium burning phase. ^{16}O (not shown in Fig. 8) and ^{12}C are the most abundant isotopes. The initial ^{12}C is rather rapidly converted by the ^{12}C+^{12}C fusion process to ^{20}Ne as outlined above. Additionally, ^{24}Mg is also formed and becomes highly abundant toward the end of the carbon burning phase. This is associated with a partial production of ^{28}Si. These processes depend on the reaction rates of ^{24}Mg(α, γ)^{28}Si and the competing ^{24}Mg(n, γ)^{25}Mg reaction.

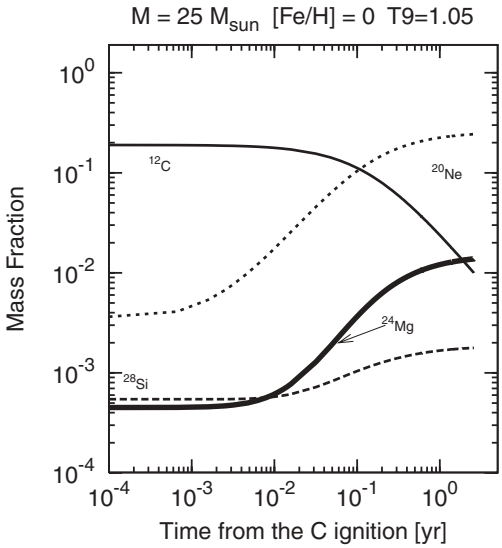

FIG. 8. Nucleosynthesis of low-Z isotopes ($Z = 6$–14) during shell carbon burning in a low metallicity $25M_{\odot}$ star.

VI. SUMMARY AND CONCLUSION

This paper describes a measurement of the ^{24}Mg(α, γ)^{28}Si reaction in the energy range of stellar carbon burning. Previously measured resonances have been confirmed, and several new resonances have been investigated above 1.0 MeV α energy. The present reaction rate confirms previous predictions [10,11], but the new data considerably reduce the uncertainties associated with these previous estimates. This is necessary for achieving more reliable predictions for the detailed nucleosynthesis pattern associated with stellar carbon burning. The yield measurements at the lowest energies were clearly handicapped by radiation background. This is the main limitation to exploring the reaction toward lower energies. New techniques need to be developed to pursue such low energy measurements for this and other α capture reaction measurements of relevance for stellar helium burning and carbon burning. Alternative techniques are either experiments in an underground environment that helps reduce the cosmic-ray-induced background radiation by passive shielding [22] or inverse kinematics experiments at recoil separators to select reaction events only by rejecting background-induced events by active shielding techniques [23]. Low energy studies do, however, require large acceptance separators, which will hopefully become available in the near future [24].

This is not only important for the measurement of α capture reactions on light nuclei ($Z \leqslant 10$) of relevance in stellar helium burning but also for a number of α capture reactions on heavier nuclei ($Z \geqslant 10$) as demonstrated in the simulation of shell carbon burning discussed herein. These simulations underline the relevance of α capture reactions in carbon burning. This is strongly correlated with the strength of the ^{12}C(^{12}C,α)^{20}Ne reaction channel providing the necessary α flux [21]. We demonstrated in this paper that while ^{24}Mg is produced by the subsequent ^{20}Ne(α, γ)^{24}Mg reaction, the depletion of ^{24}Mg is dominated by neutron capture rather than α capture, shifting the Mg isotopic abundance ratios. In general, however, these simulations underlined the importance of detailed α, proton, and neutron capture reaction measurements in the Ne to Si range to allow a consistent and reliable prediction of the nucleosynthesis and final abundance pattern in shell carbon burning.

ACKNOWLEDGMENTS

This work was supported by the National Science Foundation under Grant No. PHY01-40324 and the Joint Institute for Nuclear Astrophysics, NSF-PFC, under Grant No. PHY02-16783. One of the authors, M.P., was also supported by a Marie Curie International Reintegration Grant within the 6th European Community Framework Programme, Grant No. MIRG-CT-2006-046520.

[1] P. J. M. Smulders and P. M. Endt, Physica **28**, 1093 (1962).
[2] P. B. Lyons, Nucl. Phys. **A130**, 25 (1969).
[3] P. M. Endt, Nucl. Phys. **A633**, 1 (1998).
[4] B. M. Paine and D. G. Sargood, Nucl. Phys. **A331**, 389 (1979).
[5] J. Brenneisen, D. Grathwohl, M. Lickert, R. Ott, H. Röpke, J. Schmälzlin, P. Siedle, and B. H. Wildenthal, Z. Phys. A **352**, 149 (1995).
[6] J. W. Maas, E. Somorjai, H. D. Graber, C. A. van den Wijngaart, C. van der Leun, and P. M. Endt, Nucl. Phys. **A301**, 213 (1978).
[7] National Nuclear Data Center, http://www.nndc.bnl.gov/nudat2/, information extracted from the NuDat 2 database.
[8] P. M. Endt, Nucl. Phys. **A521**, 1 (1990).
[9] J. F. Ziegler and J. P. Biersack, SRIM–the stopping and range of ions in matter (computer software).
[10] G. R. Caughlan and W. A. Fowler, At. Data Nucl. Data Tables **40**, 283 (1988).
[11] T. Rauscher, F.-K. Thielemann, J. Görres, and M. Wiescher, Nucl. Phys. **A675**, 695 (1988).
[12] S. O. Limongi and M. A. Chieffi, Astrophys. J. Suppl. Ser. **129**, 625 (2000).
[13] M. F. El Eid, L. S. The, and B. S. Meyer, Astrophys. J. **655**, 1058 (2007).
[14] M. Pignatari, R. Gallino, C. Baldovin, M. Wiescher, F. Herwig, A. Heger, M. Heil, and F. Käppeler, in *Proceedings of Nuclei in the Cosmos IX, June 25–30, 2006,* Proceedings of Science NIC-IX (2006), 061.
[15] C. Raiteri, M. Busso, R. Gallino, and G. Picchio, Astrophys. J. **371**, 665 (1991).
[16] C. Angulo, M. Arnould, M. Rayet, P. Descouvemont, D. Baye, C. Leclercq-Willain, A. Coc, S. Barhoumi, P. Aguer, C. Rolfs *et al.*, Nucl. Phys. **A656**, 3 (1999).
[17] I. Dillmann, M. Heil, F. Käppeler, R. Plag, T. Rauscher, and F.-K. Thielemann, AIP Conf. Proc. **819**, 123 (2006).
[18] S. Woosley, A. Heger, and T. Waever, Rev. Mod. Phys. **74**, 1015 (2002).
[19] F.-K. Thielemann and W. Arnett, Astrophys. J. **295**, 604 (1985).
[20] A. Chieffi, M. Limongi, and O. Straniero, Astrophys. J. **502**, 737 (1998).
[21] M. Pignatari (in preparation).
[22] A. Formicola, G. Imbriani, M. Junker, D. Bemmerer, R. Bonetti, C. Broggini, C. Casella, P. Corvisiero, H. Costantini, G. Gervino *et al.*, Nucl. Instrum. Methods A **507**, 609 (2003).
[23] D. Schürmann, A. Di Leva, L. Gialanella, D. Rogalla, and F. Strieder, Eur. Phys. J. A **26**, 301 (2005).
[24] M. Couder, G. P. A. Berg, J. Görres, P. J. LeBlanc, L. O. Lamm, E. Stech, M. Wiescher, and J. Hinnefeld, Nucl. Instrum. Methods A **587**, 35 (2008).